Appl. Phys. B 87, 749–754 (2007)
DOI: 10.1007/s00340-007-2642-6

Applied Physics B
Lasers and Optics

J.-F. DAIGLE[1,✉]
G. MÉJEAN[1]
W. LIU[1]
F. THÉBERGE[1]
H.L. XU[1]
Y. KAMALI[1]
J. BERNHARDT[1]
A. AZARM[1]
Q. SUN[1]
P. MATHIEU[2]
G. ROY[2]
J.-R. SIMARD[2]
S.L. CHIN[1]

Long range trace detection in aqueous aerosol using remote filament-induced breakdown spectroscopy

[1] Centre d'Optique, Photonique et Laser (COPL) et le Département de Physique, de Génie Physique et d'Optique, Université Laval, Québec, Québec, Canada, G1K 7P4
[2] The Sensing (Air & Surface) & Optronics Section of the Defense Research and Development Center, Valcartier, QC, Canada, G3J 1X5

Received: 1 December 2006/Revised version: 14 March 2007
Published online: 17 May 2007 • **© Springer-Verlag 2007**

ABSTRACT Remote filament induced breakdown spectroscopy (R-FIBS) is used for probing a cloud of microdroplets where table salt has been dissolved. These microdroplets are a good simulant for aerosols. We demonstrated experimentally that R-FIBS can efficiently be used as a ppm-level sensing technique to remotely retrieve the composition of microdroplets in clouds located at a distance. The technique has been successfully tested up to 70 m and, as revealed by extrapolation, showed great potential for kilometer-range application. The proposed technique is sensitive to the solvent as well. For the first time, to the best of our knowledge, four hydrogen bands from the Balmer series were observed in an aqueous microdroplet cloud after H_2O molecules were broken by the light filaments.

PACS 42.62.Fi; 92.20.Bk; 95.75.Qr

1 Introduction

Remote, real-time detection of atmospheric aerosols has become a critical issue for both environmental and security/defense purposes. In the former case, the development of global climate models through total characterization of atmospheric clouds cannot be achieved without determining the composition of the water microdroplets and other aerosols [1]. The latter, motivated by security concerns, is in need of new techniques to efficiently monitor ambient aerosols that could contain toxic chemical or biological agents. A first aim is not to be able to identify the probed aerosols, but to be able to give an efficient alarm for potentially dangerous clouds of aerosols as far as possible.

At small distances, nanosecond laser-induced breakdown spectroscopy (ns-LIBS) has proven its feasibility on aqueous calcium aerosols [2]. However, it seems very difficult to extend this technique to remote sensing purposes. Indeed, because of diffraction, it becomes unrealistic to deliver enough intensity at a far distance to create a plasma. This limitation can be circumvented by the use of femtosecond terawatt laser pulses. The propagation of such laser pulses in air is dominated by nonlinear effects which result in the formation of a self-guided structure that is called a filament. This filament appears as a dynamic equilibrium between Kerr self-focusing and self-defocusing by the self-generated low-density plasma produced by multiphoton/tunnel ionization of the air molecules [3]. Moreover, filaments have a clamped intensity of approximately 5×10^{13} W/cm^2 in air [4] that is high enough to ionize molecules. Moreover, filaments have been observed as far as 2 km [5]. Because the high intensity inside the filament is clamped, the fluorescence signals of molecules inside the filament column are rather uniform throughout the entire filament volume [6–8]. Remote filament induced breakdown spectroscopy (R-FIBS) has already demonstrated its efficiency on metallic [8] and solid biological [9] samples. The Teramobile group demonstrated that on copper and steel targets [8] the detection technique was very promising for kilometer-range applications. In addition, terawatt femtosecond laser pulses successfully excited fluorescence from gaseous [6, 10] targets in femto-LIDAR configuration. R-FIBS thus represents an attractive candidate for time-resolved remote sensing of atmospheric aerosol constituents.

Favre et al. [10] demonstrated that microplasma can be formed in microdroplets thanks to filament interaction with aerosols and the Teramobile group also reported several filament–aerosol interaction experiments [12–14]. They showed that, as long as the transmitted power of the whole beam is higher than the critical power, filaments can survive the interaction with aerosols. Another one was especially dedicated to broadband two-photon laser-induced fluorescence (LIF) measurements on bioaerosols [15]. Recently, Fujii et al. demonstrated that sodium atomic lines could be observed using R-FIBS in aerosols [16]. The authors focused 130-mJ compressed pulses of 70 fs with a 20 m concave mirror on a thick aerosol target. They were able to detect sodium fluorescence in a cloud of 300 g/L salt concentration positioned 18 m away from the focusing mirror. This concentration roughly corresponds to the concentration of the Dead Sea [17].

✉ Fax: +1-418-656-2623, E-mail: jfdaigle2@yahoo.ca

In the present work, using a similar technique but with a special focusing telescope that allows the control of filaments at long distances [6], we demonstrated that ppm-level sodium can efficiently be excited and observed 70 m away from the detection system. Also, in comparison with the previous study of Fujii et al. [16], the threshold for salt concentration is reduced by four orders of magnitude. It is interesting to note that the four main atomic hydrogen spectral bands from the Balmer series were also detected. This indicates that the breakdown of the water droplets into atomic species occurred. This latter observation and the capability to detect diluted species inside the aerosol to ppm levels strongly increase the potential of R-FIBS for aerosol detection.

2 Experiments and results

The experiments were performed with the setups shown in Fig. 1. Laser pulses, centered at 800 nm, were emitted with a 10-Hz repetition rate by a chirped pulse amplification (CPA) Ti:sapphire laser system. They were focused using a variable focal length telescope consisting of a 5-cm-diameter convex mirror with $f = -50$ cm and an 8-cm-diameter converging lens with $f = 100$ cm mounted on a translation stage. In order to reduce white-light generation through self-phase modulation [18] and create strong constructively competing short filaments, the telescope is specially designed to always keep the self-focus close to the geometrical focus [6]. Pulse duration could be varied by changing the distance between the compressor grating pair and the pulse energy is adjusted with a half-wave plate and polarizer.

Aerosol was generated in the same way as Fujii et al. [16] by using a commercial ultrasonic humidifier (Sunbeam, Health at Home) and injected into a mobile aerosol chamber. The aqueous solution is made from a de-ionized water solvent in which the appropriate quantity of salt is added. Since the droplet size generated by a similar aerosol source has been measured by Fujii et al. [16], we assume that our droplets also have a mean radius of 5 μm. In the first part of the experiments, a 75 cm open ended cylindrical plastic pipe, used as a concentrator, is placed inside the chamber to increase the droplet density. The aerosols traveled from the humidifier to the plastic pipe via a flexible canalization. In order to avoid laser beam scattering by the droplets before the target, an 8-cm-diameter ventilator, located just below the entrance of the pipe, blows the excess aerosol leaving the plastic pipe away from the laser path (Fig. 1a). It ensured that, at the entrance of the pipe, the laser pulse would interact with a practically flat and thick aerosol fog. In these conditions, the cloud's optical density is characterized by the complete attenuation of a continuous-wave 15-mW He-Ne laser beam propagating over 75 cm. Later, to demonstrate the feasibility for real atmospheric applications, the droplet concentration is decreased by removing the plastic pipe. In this case, the He-Ne laser beam transmission, propagating over 120 cm, is 72%. This roughly corresponds to a droplet concentration of 1700 cm^{-3}, which is approximately 10 times the concentration of the thinnest natural cloud [19]. At all times, in order to avoid laboratory contamination, a flexible plastic pipe connects the chamber to the building's ventilation system and sucks the aerosol away. The negative pressure inside the chamber prevented the excess aerosol from escaping from the chamber into the laboratory.

In the experiment, the aerosol chamber was located at different distances (5 m to 70 m) away from the sending telescope (Fig. 1a). Beside the telescope, a typical UV fiber coupled LIDAR setup [6] collected the R-FIBS spectra. The

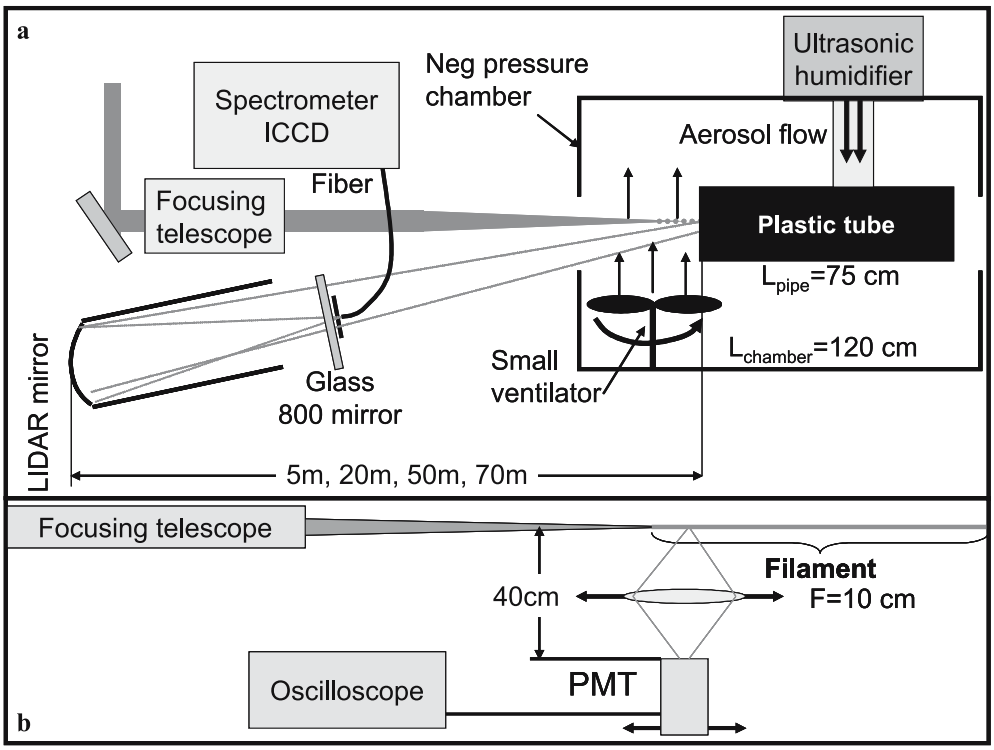

FIGURE 1 Experimental setups for (**a**) spectral characterization of aerosols and (**b**) filament side characterization via molecular nitrogen fluorescence

1-m-focal length LIDAR mirror has 30-cm diameter. The collected signal was delivered to a SpectraPro-500i SP-558 spectrometer equipped with a PIMAX:512 ICCD (intensified charge-coupled device) camera. For each experimental condition, the Na fluorescence signal was optimized by adjusting the effective focal length of the sending telescope [6].

To show that the interaction with the aerosol involves filamentation, we measured the nitrogen fluorescence typically emitted from inside a filament [20]. Figure 1b shows the experimental setup. For this part of the experiment, the aerosol chamber was removed. A scanning unit, consisting of a fused-silica 10-cm-focal length lens and a photomultiplier tube (PMT) with UG11 filter in a one to one imaging configuration, was moved parallel to the direction of the filament to measure the nitrogen fluorescence distribution from inside the filament as a function of the distance from the LIDAR's output mirror. The distance between the PMT and the filament was 40 cm.

The spectrum presented in Fig. 2 is the result of a 100-shot accumulation. It was measured in thick-fog conditions, which means that the pipe was inside the chamber. The corresponding laser pulse duration was negatively chirped to 80 fs with 70-mJ pulse energy. The distance from the pipe entrance to the last lens of the focusing telescope was 3.5 m and 5 m to the LIDAR mirror. The gate of the ICCD camera was opened for 500 ns, 8 ns after the laser pulse had arrived at the pipe entrance. In addition to the strong sodium fluorescence, we observed, for the first time in aerosols, the presence of the four main atomic hydrogen fluorescence bands of the Balmer series which are the result of seven atomic transitions [21]. The first H I_α line is very strong while the rest of the lines are rather weak. This Balmer series proves that the laser pulses induce breakdown of the droplets and H_2O molecules. The fact that the aqueous medium can be detected opens up a way for solvent identification. The plot presented as the inset of Fig. 2 shows the results obtained using the filament-scanning setup shown in Fig. 1b. The solid line indicates the position of the aerosol pipe entrance. It shows a $\sim$ 50 cm long plasma column penetrating into the pipe for 20 cm. This firmly indicates that the interaction involved filamentation. The characteristic plasma distribution of the filament shows two spatially separated nitrogen fluorescence signals. Because of the very high

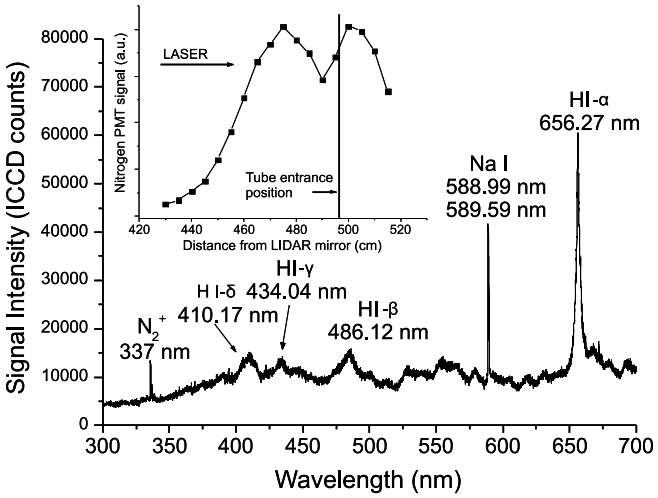

FIGURE 2 Typical spectrum measured 5 m from the LIDAR mirror with 80-fs negatively chirped pulses of 72 mJ. *Inset*: filament-generated plasma distribution position with respect to aerosol pipe entrance

input peak power (850 GW after the sending telescope), this phenomenon is related to refocusing [22] as well as multiple filamentation [23].

Figure 3 shows the effect of pulse duration on the two major spectral lines. Both sodium and hydrogen emissions increase with pulse duration. This implies that, in order to enhance fluorescence signals, longer pulses are required to heat and accelerate electrons through the inverse bremstralhlung effect. Due to this acceleration, avalanche ionization [24] occurs and produces water droplet breakdown. While transform-limited pulses of 47 fs could excite rather strong sodium fluorescence, longer pulses are needed to excite hydrogen lines. This means that avalanche ionization's involvement in the fluorescence mechanism for hydrogen is more important than for sodium. However, it was found that, for both systems, the signal increased with pulse duration up to a certain limit, which is similar in the cases of both sodium and hydrogen ($\sim$ 80 fs), and then decreases for longer negative chirp. In fact, pulses with longer durations have lower peak powers. Such pulses generate a smaller number of filaments. Since, in our experiment, fluorescence is induced by filamentation, a decrease in

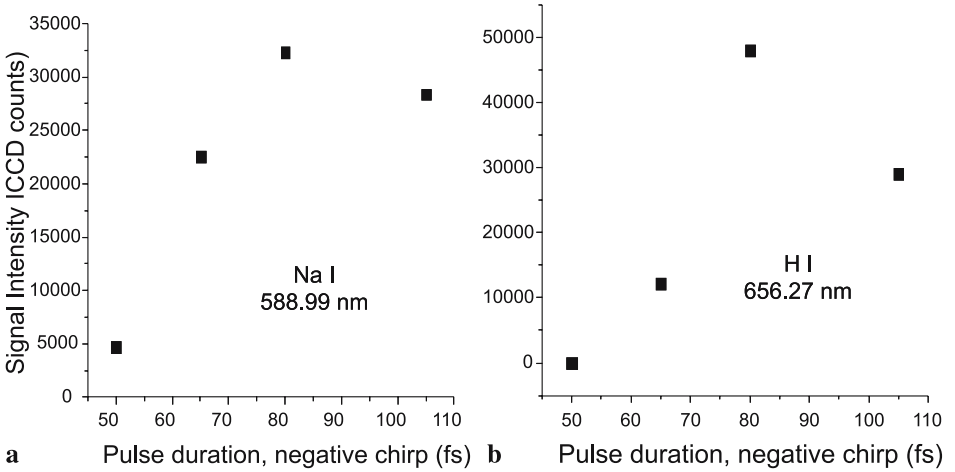

FIGURE 3 (**a**) Sodium signal intensity as a function of negative chirp at 5 m. (**b**) Hydrogen signal intensity as a function of negative chirp at 5 m

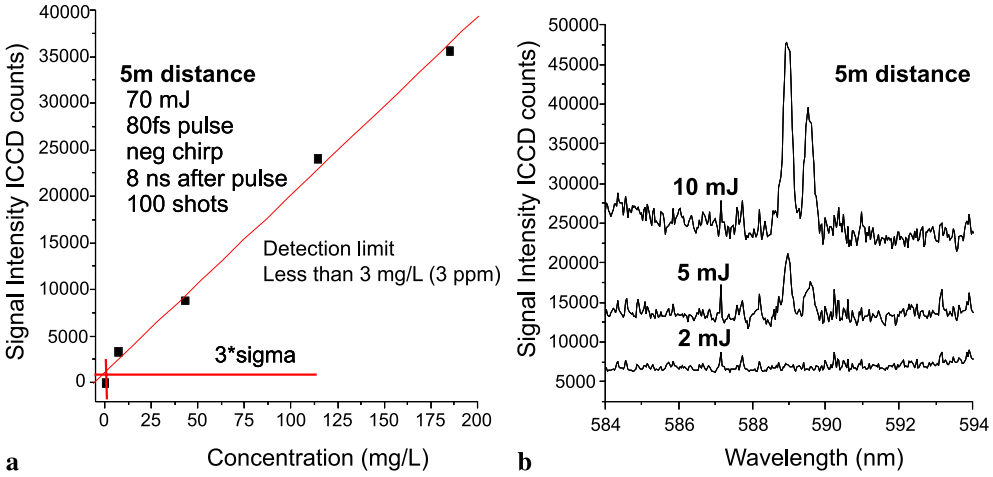

FIGURE 4 (**a**) Sodium signal intensity as a function of salt concentration at 5 m. (**b**) Low-energy sodium excitation

the number of filaments reduces the number of water droplets' breakdown events resulting in a weaker R-FIBS signal. This suggests that the optimum aerosol interaction seems to be a compromise between longer pulses' avalanche ionization and multiple filamentation from high peak power pulses.

At 5 m, we measured the detection limit of this technique. First of all, with 70-mJ compressed pulse energy, the signal could be observed at a salt concentration as low as 7 mg/L (7 ppm). As shown in Fig. 4a, a linear extrapolation to the 3σ level (where σ is the standard deviation of the signal) demonstrates that the detection limit is inferior to 3 ppm. Secondly, at a concentration of 300 mg/L, sodium fingerprint fluorescence could be distinguished with 80-fs chirped pulses of 5 mJ each (Fig. 4b). In fact, below this energy, it was impossible to generate strong filaments.

The plastic pipe was removed from the chamber and the droplet concentration was characterized with a 72% transmission of the He-Ne laser beam. Under this condition, the lowest salt concentration at which the sodium lines could be observed, with 70-mJ pulses, was 10 mg/L. When the salt concentration was increased to 20 g/L, two other atomic sodium lines were observed at 568.263 nm and 568.821 nm [21]. Finally, 300 mg/L of salt can still be detected with 10-mJ pulses.

Using the same setup as in Fig. 1a with the plastic pipe in place, we performed the manipulations in a corridor next to the laboratory. Three different chamber positions were considered: 20 m, 50 m and 70 m from the LIDAR mirror. A 5 g/L salt solution was used. In order to avoid early filamentation in the 10-m tube linking the corridor to the laboratory, negatively chirped 10 ps/72 mJ pulses were launched. Because of the lower peak power (6.8 GW after the sending telescope), the long pulse duration used in this configuration made impossible the observation of the hydrogen lines, even at 20 m. The signal intensity plotted in Fig. 5 as a function of distance reveals that, at 70 m, the signal is still above the 3σ limit and the lines are easily distinguished from the background (inset of Fig. 5). Even if the sending telescope's property of generating short and intense filaments cannot be questioned at small distances, the lack of large focusing optics to further increase the beam size for long propagation reduced the sodium detection efficiency. In fact, since the self-focusing distance is proportional to the square of the beam diameter [25], at long focusing ranges the distance between the geometrical focus

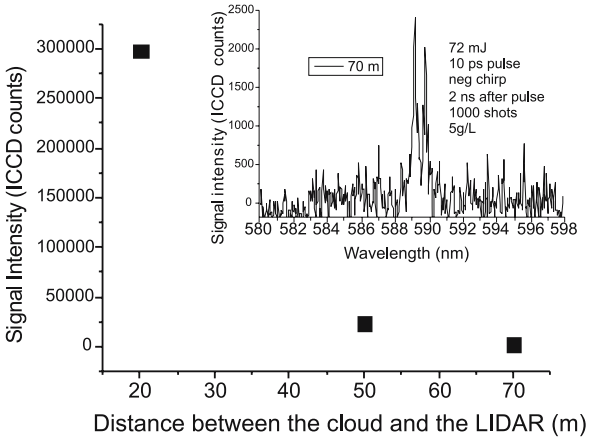

FIGURE 5 Sodium signal as a function of distance from the LIDAR mirror. *Inset*: sodium signal captured with the aerosol chamber positioned 70 m from the LIDAR mirror

and the self-focus point is reduced. This effect reduces the constructive interference of the multiple filaments, which in turn reduces the ionization efficiency. As a result, in addition to the classical $1/R^2$ solid-angle factor, the captured signal intensity was influenced by the decrease of filament plasma density with increasing focal length of the telescope [6, 7]. In our experiments, sodium was detected from up to 70 m away from the sending telescope. In principle, it is possible to generate intense filaments at km range based upon the current telescopic design [6]. This will thus help pushing R-FIBS to km-range remote detection.

The mobile chamber was then positioned 50 m away from the LIDAR. The salt concentration was gradually decreased to test the detection limit. The results are presented in Fig. 6. The linear behavior allows the determination of the 3σ detection limit. It was found that, at 50 m, the limit is around 33 ppm. This result demonstrates the great potential of the technique for long-distance trace measurements in aqueous aerosols.

Finally, sodium fluorescence from a thin fog characterized with 86% transmission of a He-Ne laser beam and a salt concentration of 1.25 g/L is measured with the chamber positioned 50 m away from the LIDAR mirror. This value of the transmission of the He-Ne laser beam indicates that the droplet concentration is roughly 1000 cm^{-3} [19]. It has been

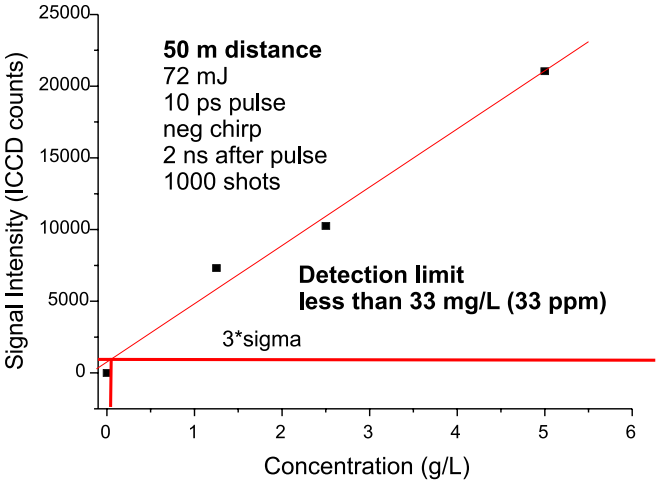

FIGURE 6 Fluorescence signal as a function of salt concentration at 50 m

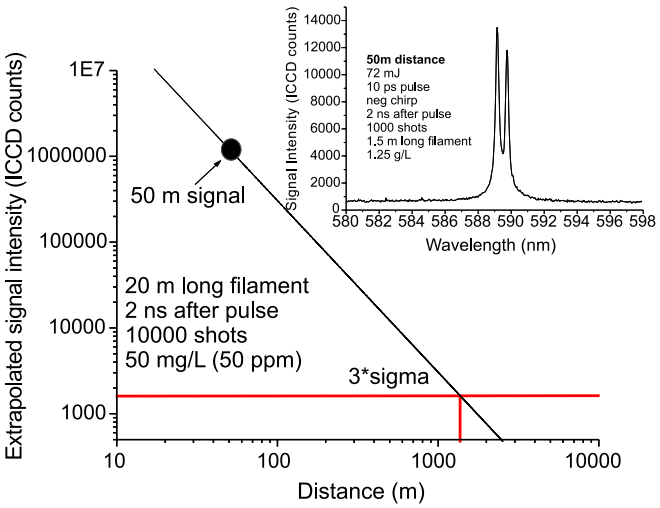

FIGURE 7 Extrapolation on distance based on a signal collected from a thin cloud at 50 m. *Inset*: thin cloud signal at 50 m used for the extrapolation

reported that filaments can transmit through clouds of optical thickness of up to 3.2 [13]. This value has been measured over 0.35-m aerosol fog using He-Ne laser beam transmission and corresponds to a cloud of droplet density of the order of 10^5 cm^{-3}. It was also concluded that the femtosecond laser pulses can propagate unaffected through a cloud of optical thickness of 1.2 for 0.35 m and still generate filaments [14]. In our experiment, the He-Ne laser beam is transmitted at 86% and, thus, filaments can penetrate the cloud and excite the sodium fluorescence. In these conditions, unlike thick clouds, at which only a small portion of the filaments interacted with the aerosols, the signal now comes from the entire filament length. The amount of fluorescence captured increases with the size of the interaction volume. So, in thin clouds, filament transmission would lead to an enhanced R-FIBS signal.

3 Discussion

Because of the above-mentioned argument [14], the measured thin-fog signal is used to make an extrapolation over distance. Our calibration point is the signal measured from 50 m away under the following conditions: salt concentration, 1.25 g/L; He-Ne laser beam transmission, 86%; filament length, 1.5 m and a 1000 laser shot accumulation. In these conditions, the spectrum is shown as the inset of Fig. 7. The signal concentration dependence plot in Fig. 6 and the LIDAR equation $I \propto L/R^2$ (where I is the signal intensity, L the effective filament length and R the distance between the end of the filament and the detector) [15] is used to extrapolate this result over distance. We estimate that, for a filament length of $L = 20$ m, the signal detection limit of three standard deviations will be reached, with a 10 000-shot accumulation, slightly beyond 1.25 km. The extrapolated curve is shown in Fig. 7, where the black dot represents the calibration point. It is possible to generate such a filament at these distances. However, to achieve this kilometer-range detection limit requires control over the onset of the filaments. As previously mentioned, this obstacle could be circumvented using an appropriate telescopic system as a beam focusing device [6]. Since the closest clouds, Cumulus humilis, are located around 500–1000 m over sea level [26], this result opens a way for efficient ppm-level remote sensing of atmospheric aerosols in air.

Before ending, we would like to comment upon the strong discrepancy between these results and those obtained by Fujii et al. [16]. There was essentially no difference between our experiment and that of Fujii except that we used a control focusing telescope as a laser beam sending device. In our experiment, with half the pulse energy and a salt concentration lowered by 60 times, approximately the same signal was recovered, but at a distance more than three times longer. It appears that, at high energies, in the case of Fujii et al., beam profile inhomogeneity and early self-focusing conditions lead to multi-filamentation competition [23] which, in turn, decreases the breakdown efficiency. The filaments obtained in the present experiment were, thanks to the focusing telescope, forced into a tight bundle and interfered constructively. In fact, a beam profile analysis showed that, at 20 m, the multiple filaments were confined to a 3 mm minimal diameter high-intensity zone around the nonlinear focal point.

4 Conclusion

In conclusion, we experimentally demonstrated the remote composition sensing of a microdroplet cloud in air by R-FIBS using terawatt pulses focused on saltwater aerosols located up to 70 m away from the LIDAR mirror. The extreme efficiency exhibited by Na fluorescence excitation, even at ppm-level salt concentrations, low pulse energies, low droplet densities and long distances, gives a good idea of the great potential of the technique for real application remote sensing of trace constituents of aerosols. Also, the presence of the four main atomic hydrogen bands from the Balmer series leads the way towards the identification of the aqueous solvent. Moreover, the extrapolated signal, based on some plausible approximations, demonstrated that it is possible to observe ppm-level concentrations up to 1.25 km. Since this value is almost twice the distance from sea level to the closest atmospheric cloud layer [27], R-FIBS represents an ideal candidate for atmospheric measurements on aerosols.

ACKNOWLEDGEMENTS This work was partially supported by NSERC, DRDC Valcartier, Canada Research Chairs, CIPI, CFI, Femtotech and FQRNT. We appreciate very much the technical assistance of Mr. Mario Martin.

REFERENCES

1 S. Borrmann, J. Curtius, Nature **418**, 826 (2002)
2 B.C. Windom, P.K. Diwakar, D.W. Hahn, Spectrochim. Acta B **61**, 788 (2006)
3 S.L. Chin, S.A. Hosseini, W. Liu, Q. Luo, F. Théberge, N. Aközbek, A. Becker, V.P. Kandidov, O.G. Kosareva, H. Schroeder, Can. J. Phys. **83**, 863 (2005)
4 A. Becker, N. Aközbek, K. Vijayalakshmi, E. Oral, C.M. Bowden, S.L. Chin, Appl. Phys. B **73**, 287 (2001)
5 M. Rodriguez, R. Bourayou, G. Méjean, J. Kasparian, J. Yu, E. Salmon, A. Scholz, B. Stecklum, J. Eislöffel, U. Laux, A.P. Hatzes, R. Sauerbrey, L. Wöste, J.-P. Wolf, Phys. Rev. E **69**, 036 607 (2004)
6 W. Liu, F. Theberge, J.-F. Daigle, P.T. Simard, S.M. Sarifi, Y. Kamali, H.L. Xu, S.L. Chin, Appl. Phys. B **85**, 55 (2006)
7 F. Théberge, W. Liu, P.T. Simard, A. Becker, S.L. Chin, Phys. Rev. E **74**, 036 406 (2006)
8 K. Stelmaszczyk, P. Rohwetter, G. Méjean, J. Yu, E. Salmon, J. Kasparian, R. Ackermann, J.-P. Wolf, L. Wöste, Appl. Phys. Lett. **85**, 3977 (2004)
9 H.L. Xu, W. Liu, S.L. Chin, Opt. Lett. **31**, 1540 (2006)
10 C. Favre, V. Boutou, S.C. Hill, W. Zimmer, M. Krenz, H. Lambrecht, J. Yu, R.K. Chang, L. Woeste, J.-P. Wolf, Phys. Rev. Lett. **89**, 05 002 (2002)
11 H.L. Xu, J.-F. Daigle, Q. Luo, S.L. Chin, Appl. Phys. B **82**, 655 (2006)
12 G. Méjean, J. Kasparian, J. Yu, E. Salmon, S. Frey, J.-P. Wolf, S. Skupin, A. Vinçotte, R. Nuter, S. Champeaux, L. Bergé, Phys. Rev. E **72**, 026 611 (2005)
13 R. Bourayou, G. Méjean, J. Kasparian, M. Rodriguez, E. Salmon, J. Yu, J. Opt. Soc. Am. B **22**, 2 (2005)
14 F. Courvoisier, V. Boutou, J. Kasparian, E. Salmon, G. Méjean, J. Yu, J.-P. Wolf, Appl. Phys. Lett. **83**, 2 (2003)
15 G. Méjean, J. Kasparian, J. Yu, S. Frey, E. Salmon, J.-P. Wolf, Appl. Phys. B **78**, 535 (2004)
16 T. Fujii, N. Goto, M. Miki, T. Nayuki, K. Nemoto, Opt. Lett. **31**, 23 (2006)
17 Wikipedia Free Encyclopedia, see http://en.wikipedia.org/wiki/Dead_Sea
18 F. Théberge, W. Liu, Q. Luo, S.L. Chin, Appl. Phys. B **80**, 221 (2005)
19 Resources in Earth Observation, see http://ceos.cnes.fr:8100/cdrom-98/astart.htm
20 A. Talebpour, M. Abdel-Fattah, A.D. Bandrauk, S.L. Chin, Laser Phys. **11**, 68 (2001)
21 NIST Database, see http://physics.nist.gov/cgi-bin/AtData/lines-form
22 A. Talebpour, S. Petit, S.L. Chin, Opt. Commun. **171**, 285 (1999)
23 Q. Luo, S.A. Hosseini, W. Liu, J.-F. Gravel, O.G. Kosareva, N.A. Panov, N. Aközbek, V.P. Kandidov, G. Roy, S.L. Chin, Appl. Phys. B **80**, 35 (2005)
24 S.L. Chin, From multiphoton to tunnel ionization, in *Advances in Multiphoton Processes and Spectroscopy*, ed. by S.H. Lin, A.A. Villaeys, Y. Fujimura (World Scientific, Singapore, 2004), Chap. 16, pp. 249–272
25 J.H. Marburger, Prog. Quantum Electron. **4**, 35 (1975)
26 Q. Luo, J. Yu, S.A. Hosseini, W. Liu, B. Ferland, G. Roy, S.L. Chin, Appl. Opt. **44**, 391 (2005)
27 Wikipedia Free Encyclopedia, see http://en.wikipedia.org/wiki/Cumulus_humilis_cloud